Observations of cross-channel structure of flow in an energetic tidal channel

Mario Cáceres
Servicio Hidrografico y Oceanografico de la Armada, Valparaiso, Chile

Arnoldo Valle-Levinson and Larry Atkinson
Center for Coastal Physical Oceanography, Department of Ocean, Earth, and Atmospheric Sciences, Old Dominion University, Norfolk, Virginia, USA

Received 11 May 2001; revised 8 July 2002; accepted 21 November 2002; published 8 April 2003.

[1] Measurements of velocity and density profiles were made to describe the transverse structure of flow in Chacao Channel, Southern Chile (41.75°S), where typical tidal velocities are ~4 m/s. Current profiles were obtained with a 307.2 kHz Acoustic Doppler Current Profiler (ADCP) over 25 repetitions of a cross-channel transect during one semidiurnal tidal cycle. The 2.2 km long transect ran northeast/southwest across the channel. A northern channel (120 m deep) and a southern channel (85 m deep) were separated by Remolinos Rock, a pinnacle that rises to 20 m depth at ~0.7 km from the southern side. Density measurements to depths of ~50 m were obtained with a Conductivity, Temperature, and Depth (CTD) recorder at the north and south ends of each transect repetition. One CTD profile was also taken in the middle of the northern channel. The mean flow exhibited weak vertical structure because of strong vertical mixing. The predominant lateral structure consisted of mean outflow (toward the ocean) in the channels and mean inflow (toward Gulf of Ancud) over the pinnacle and the sides of the channel. This lateral structure pattern was consistent with the mean flow pattern expected from tidal rectification, as robust overtides were generated throughout the transect. The contributions to flow divergence and vorticity by the lateral variations of the lateral flow ($\partial v/\partial y$) and by the lateral shears of the along-channel flow ($\partial u/\partial y$), respectively, were both of the order of 10^{-3} s^{-1}. This caused advective and frictional forces (both horizontal and vertical) to be dominant in the across-channel momentum balance, as they were more than twenty times the Coriolis acceleration. The present work then represents one of the few examples reported where lateral friction (proportional to $\partial^2 v/\partial y^2$) appears relevant to the transverse momentum balance. *INDEX TERMS:* 4223 Oceanography: General: Descriptive and regional oceanography; 4235 Oceanography: General: Estuarine processes; 4512 Oceanography: Physical: Currents; *KEYWORDS:* estuarine processes, tidal currents, fiords, Chile, South America

Citation: Cáceres, M., A. Valle-Levinson, and L. Atkinson, Observations of cross-channel structure of flow in an energetic tidal channel, *J. Geophys. Res.*, *108*(C4), 3114, doi:10.1029/2001JC000968, 2003.

1. Introduction

[2] Extremely energetic tidal channels where currents exceed 3 m/s are rare. Maximum currents of 8 m/s for Seymour Narrows in British Columbia, Canada are frequently quoted among the highest speeds measured [*Pond and Pickard*, 1998]. The common feature observed in every case of an energetic tidal channel is a high tidal range. Some of the highest tidal ranges have been reported for St. John River, Bay of Fundy, Canada [*Redfield*, 1980], Minas channel, Bay of Fundy [*Tee*, 1976], South Korea [*Wells*,1983], and St. Malo, France [*Defant*, 1961, p.377], with records of 7 m, 15 m, 5–9 m, and 8–10 m, respectively.

[3] Examples of strong tidal currents in relatively deep (>80 m) channels or fjords are unusual. Some of them may be found in southern Chile, where a characteristic fjord-like coastal morphology covering about 2000 km of the Chilean coastline shows a variety of channels connecting the open ocean to the Inland Sea (Figure 1a). One of those channels is Chacao Channel, located in the northernmost part of the region of fjords in the Chilean Inland Sea. It represents one of the two direct openings between the ocean and the Inland Sea, the other being Guafo Mouth. Chacao Channel connects the open ocean with the Gulf of Ancud in the east-west direction and is approximately 40 km long with an average width of 4 km (Figure 1b).

[4] The channel exhibits tidal currents of 3 to 4.5 m/s and tidal ranges of 5.5 to 6.0 m [*SHOA*, 1993, 1995]. These currents are developed from the differences in tidal range between the east and west ends of the channel. Tidal range enlarges as the tidal wave propagates from west to east, with a remarkable increase from ~2 m in the west side (Coro-

0148-0227/03/2001JC000968$09.00

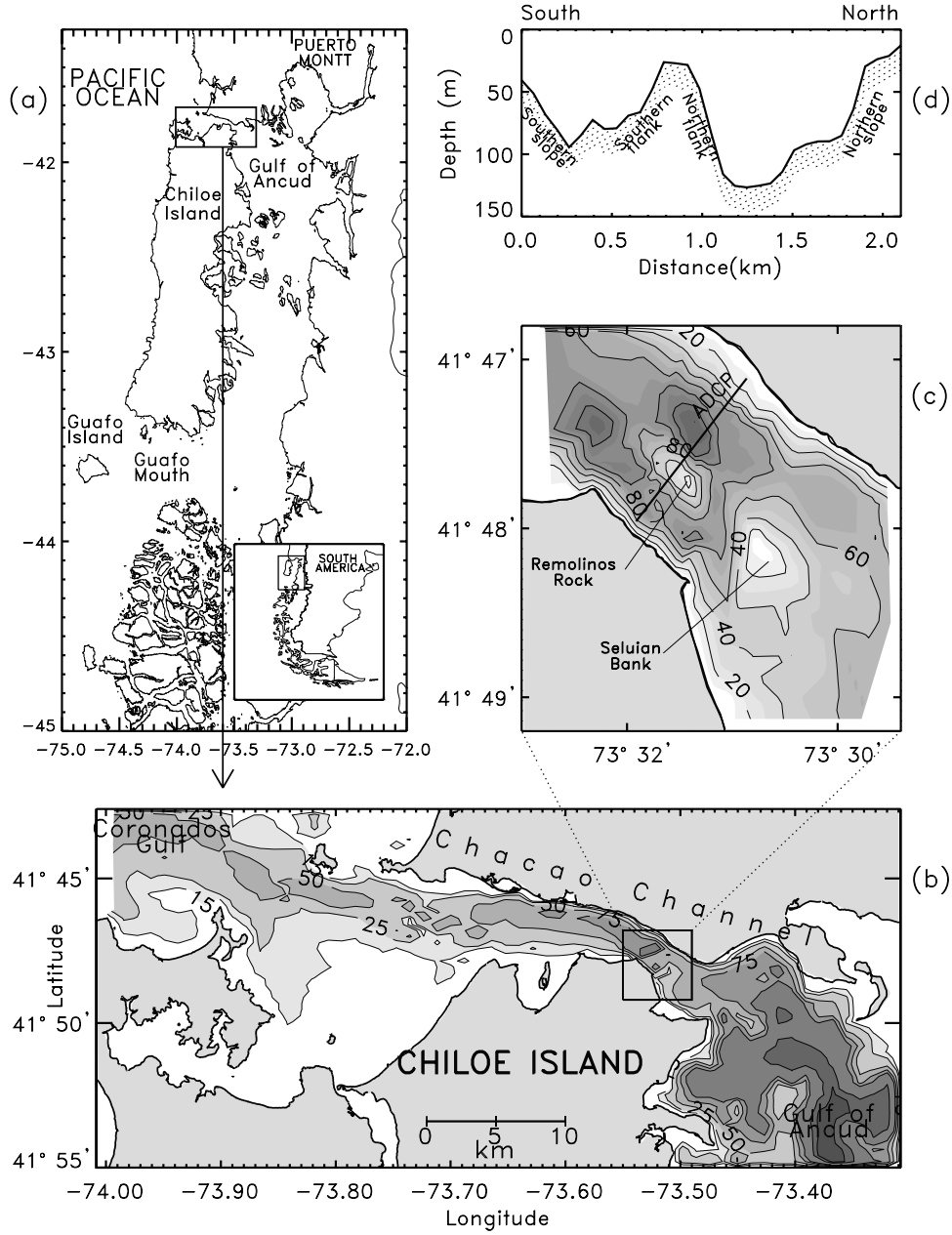

Figure 1. (a) General study area on the southern coast of Chile. (b) The measurements obtained during this experiment were made in the box shown at the narrowest part of Chacao Channel. (c) The ADCP profiles were made in the transect (∼2.2 km length) over Remolinos Rock. (d) Bottom profile associated with the ADCP transect (looking toward the ocean).

nados Gulf) to ∼6 m in the east side (Gulf of Ancud). The reason for this amplification is still under investigation, but it may be partially explained by resonant effects of the tidal wave that enters through Guafo Mouth to the south and propagates northward, along the east side of Chiloe Island up to the Gulf of Ancud. This hypothesis is supported by tidal gauge records showing a continuous increase of tidal ranges in the transit from Guafo Mouth (∼2 m) to Gulf of Ancud (∼6 m). Slack waters in Chacao Channel are brief (<15 min), and sometimes they are undetectable to the casual observer.

[5] On the basis of data obtained at Guafo Island (Figure 1a) by the Meteorological Service of the Chilean Navy (SMA), the wind regime for this region of the Inland Sea is dominated by southerly and southwesterly winds during spring and summer (October–March) and northerly and northwesterly winds during fall and winter (April–September). Northwesterly and southwesterly winds may increase the tidal current entering the channel during flood and decelerate it during ebb, enhancing sea roughness.

[6] Freshwater input to Gulf of Ancud comes from rivers draining westward from the Andes. The water circulation in Chacao Channel is weakly influenced by river flow with typical salinities during the spring season in Coronados Gulf and in the center of Gulf of Ancud in the range of 32.9–33.1 and 29.0–32.0, respectively (SHOA, personal communication, 2001).

[7] The geomorphology of Chacao Channel reflects carving by past glaciation. Its bathymetry features an isolated pinnacle around 20 m depth located at ~0.7 km from the southern side (Chiloe Island) in the narrowest part of the channel (Figures 1c and 1d). This pinnacle separates two channels, a southern channel (−85 m depth) and a northern channel (120 m depth). During very low tides, the rocks at the summit of the pinnacle may be seen above water [*SHOA*, 1995]. These rocks are called Rocas Remolinos (from spanish "eddies rocks") in nautical charts [*SHOA*, 1993]. The flanks of the pinnacle have slopes of ~16° in its northern side and ~14° in its southern side. At ~1.5 km to the southeast of Remolinos Rocks, toward the Inland Sea, is Seluian Bank (Figure 1c), which is a shoal of ~20 m depth skewed towards the southern side of the channel.

[8] In terms of the transverse dynamics in these systems, it is customary to assume an across-channel dynamic balance between the pressure gradient forces and Coriolis forces [*Dyer*, 1997], as observed by *Cameron* [1951] and *Tully* [1958] in straight fjords. This may be also appropriate for flow over low aspect ratio (vertical scale/horizontal scale) bathymetric features and relatively weak currents (<1 m/s). However, for features with high aspect ratio, where the fractional height (feature relief/water column depth) is greater than 0.7 (following *Chapman and Haidvogel* [1992]), the fluid column may be stretched and compressed, leading to relatively large velocities and particle excursions. In Chacao Channel the interaction of strong tidal currents with a pinnacle at the narrowest region of the channel suggests the generation of nonlinear tidal effects, such as overtides and bathymetrically induced flow accelerations. The stretching and contraction of streamlines around the pinnacle would invalidate the geostrophic approximation and make the frictional and advective accelerations relevant to the across-channel momentum balance. In particular, enhanced mixing processes would dominate stratifying tendencies. Overtides, which are harmonic motions with higher frequencies than the semidiurnal, may be caused by nonlinear accelerations and frictional terms [*LeBlond*, 1991]. The source terms for quarter-diurnal tides (e.g., M_4) usually arise from nonlinearities in the continuity equation, advection, and the depth effect on bottom friction; while the sixth-diurnal tides (e.g., M_6) are forced mainly by terms from bottom friction [*Parker*, 1991; *Walters and Werner*, 1991]. In any case, overtides indicate predominance of nonlinear effects.

[9] This study quantifies and describes the transverse variability produced by the interaction of strong tidal currents with a pinnacle in the middle of a channel. It presents estimates of key terms in the across-channel momentum balance to assess the validity of the geostrophic approximation.

2. Data Collections and Processing

[10] A 307.2 kHz RD Instruments ADCP and a Trimble Global Positioning System (GPS) interfaced to a laptop computer were used to obtain velocity profiles in the sampling area during one complete semidiurnal tidal cycle on 7 October 1998, 3 days after secondary neap tides (the weakest neap tides of the month). The ADCP was mounted on a catamaran ~1.2 m long, which was towed from the starboard side of the diving boat "Virago" at approximately 2.5 m/s. An average current profile consisted of 8 pings averaged every 30 s. An across-channel transect (Figure 1c) was traversed 25 times during the 12.5 hours of data collection. The ADCP data were calibrated according to *Trump and Marmorino* [1997], and bad data were removed following the procedure explained by *Valle-Levinson and Atkinson* [1999]. After the heading correction was applied, the data were rotated 13° clockwise to an along- (u flow) and across- (v flow) channel coordinate system. This was the direction of greatest variability of the tidal currents and of weakest across-channel tidal flows. CTD stations were made at the end of each transect and at a deeper (ca. 120 m) station in the channel. The present work was carried out during calm wind conditions.

[11] The semidiurnal tide (represented by the M_2 constituent) and its harmonic overtides (represented by the M_4 and M_6 constituents) were separated from the observed flow components using sinusoidal least squares regression analysis [e.g., *Lwiza et al.*, 1991]. The overtides were obtained for a preliminary assessment of nonlinear influences to the momentum balance. The root-mean-squared (rms) errors of the least-square fits were between 0.2 and 0.5 m/s and the mean error was about 0.3 m/s. This was between 5 and 10 % of the currents observed.

[12] After determining the relevance of nonlinear influences through overtides, the relative magnitude of the advective and frictional terms was compared to that of the Coriolis accelerations. To do this, a right-hand coordinate system was adopted for which y (across-channel direction) was positive toward 13° true and x (along-channel direction) was positive to 103° true. It followed that the along-channel and across-channel components of the velocity were given by u and v, respectively. In the across-channel direction the mean, averaged over a tidal cycle, momentum balance can then be given by

$$\langle u(\partial v/\partial x)\rangle + \langle w(\partial v/\partial z)\rangle + \underline{\langle v(\partial v/\partial y)\rangle} + \underline{\langle fu\rangle} = -\langle 1/\rho(\partial p/\partial y)\rangle + \langle A_h(\partial^2 v/\partial x^2)\rangle + \underline{\langle A_z(\partial^2 v/\partial z^2)\rangle} + \underline{\langle A_h(\partial^2 v/\partial y^2)\rangle} \quad (1)$$

where $v(\partial v/\partial y)$ is representative of the advective term, fu is the Coriolis term ($f = 9.7 \times 10^{-5}$ s^{-1}), $1/\rho(\partial p/\partial y)$ is the pressure gradient term (ρ = seawater density), $A_z(\partial^2 v/\partial z^2)$ is the vertical frictional term, $A_h(\partial^2 v/\partial y^2)$ is the horizontal frictional term, and brackets (< >) denote tidal averages. The terms appearing underlined were those of the complete momentum balance that could be reliably approximated.

[13] The magnitudes of each term were used to compare their relative contribution to the momentum balance in the across-estuary direction. A constant vertical eddy viscosity $A_z = 0.01$ m^2/s was used following estimates of *Bowden and Hamilton* [1975], *Csanady* [1975], *Ott and Garrett* [1998], and *Geyer et al.* [2000]. Also a constant horizontal eddy viscosity $A_h = 90$ m^2/s was used following estimates of *Smith* [1996] and *Pingree and Maddock* [1978]. Both A_z and A_h are probably underestimated relative to the strong tidal currents observed here. Although A_z and A_h are expected to change in space and time, constant values were used here for diagnostic purposes and to facilitate the calculations.

3. Results

[14] This section presents the across-channel distribution of the mean and tidal flows for the period of observation. It

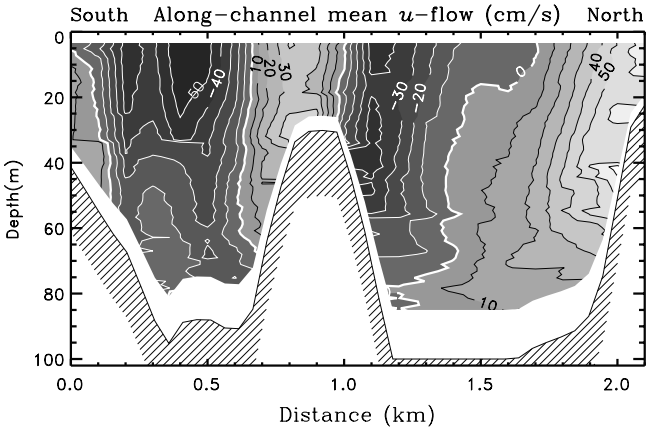

Figure 2. Across-channel distribution of the along-channel mean flow (looking toward the ocean). The mean flow showed a transverse structure where inflows (lighter) were observed over the shallow regions and outflows (darker) over the southern channel and northern flank of the Remolinos Rock.

also describes the time evolution of vertical salinity profiles made at the extremes of the ADCP transect and a vertical density profile made in the middle of the northern channel to illustrate stratification conditions. Additionally, it presents the magnitudes and across-channel distributions of the terms indicated in equation (1), with exception of the pressure gradient term. A comparison among the magnitude of various terms is shown at the end.

3.1. Mean Flow

[15] The along-channel mean flow over the period of observations is shown in Figure 2. The flow structure was significantly influenced by bathymetry. Inflows were located over the slopes and over the top and southern flank of the pinnacle. Outflows were observed over the southern channel and over the northern flank of the pinnacle. The pinnacle seemed to play a role in determining this distribution. The mean flow might be attributed to nonlinearities in the dynamics of tidal flow as indicated by the theoretical results of *Li and O'Donnell* [1997]. They found that exchange flows were correlated with topography in such a way that mean landward flows occurred over the shoals and seaward flows in the channels. The mean flow in Chacao Channel also resembled the mean flow in North Inlet, a strongly frictional tidal channel in South Carolina, USA [*Kjerfve and Proehl*, 1978]. In addition, the mean flow in Chacao Channel exhibited weak vertical structure dominated by strong lateral shears ($\partial u/\partial y$). Over the sloping bathymetry the lateral shears were comparable to the vertical shears. Maximum mean velocities were about 60 cm/s in the northern slope, comparable to the 76 cm/s observed in Minas Channel, a tidal channel with currents of 5.6 m/s [*Tee*,1976]. Although the diurnal tidal contribution (which was unresolved by the sampling) could have biased the mean flow, it is expected that the pattern will persist because of its consistence with theoretical results.

[16] The mean v flow (Figure 3a) exhibited a mean absolute magnitude in the section of about ~9 cm/s, which was almost one half of the mean value (~22 cm/s) of the along-channel mean flow (Figure 2). It also showed five changes of direction near the surface from north (positives) to south (negatives) in just 2 km, thus determining regions of strong convergence and divergence dominating the upper 40 m. This was more clearly seen in the distribution of the transverse gradients $\partial v/\partial y$ (Figure 3b). Two strong changes in direction (negative values, darker tones) are observed on both flanks of the pinnacle, while sudden increases in v velocity (positive values, lighter tones) are represented by the gradients over the southern slope and over the pinnacle. The magnitude of these gradients is up to $\sim 10^{-3}$; that is, they are one order of magnitude greater than those reported for example in the lower Chesapeake Bay [*Valle-Levinson and Atkinson*, 1999]. Magnitudes of the lateral variations of the v component were comparable in some regions of the section to those of the vertical variations $\partial v/\partial z$ (not plotted here).

3.2. Tidal Current Amplitudes

[17] The distribution of the semidiurnal tidal current amplitude (Figure 4a) showed the highest velocities centered at mid-depth in the southern channel (~3.2 m/s) and near surface in the northern channel (~3.4 m/s). Effects of bottom friction were evident as velocities decreased near the bottom and over shallow areas. Similarly to the mean flow, the lateral variations were larger than the vertical variations. In general this was also the case for the distribution of the quarter-diurnal (Figure 4b) and sixth-diurnal (Figure 4c)

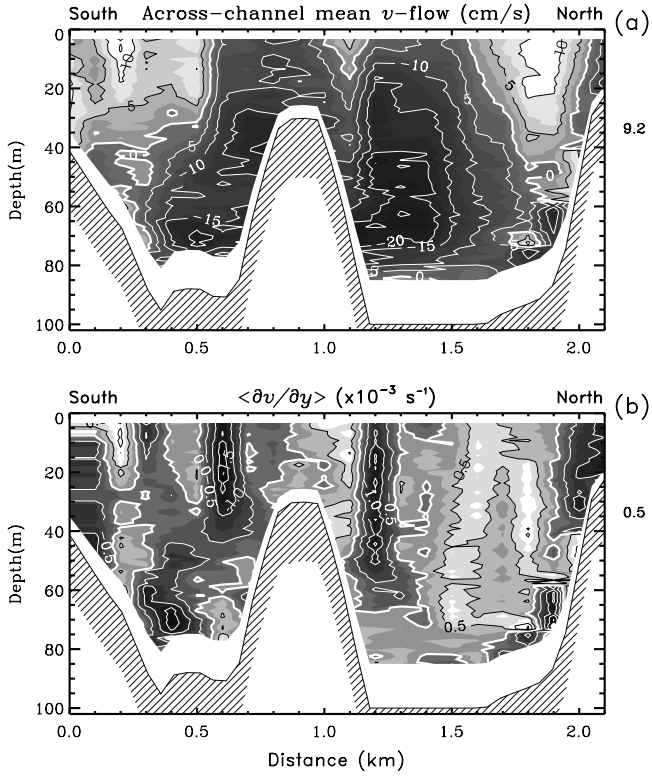

Figure 3. (a) Across-channel component of the mean flow. Positive values indicate currents to the north and negatives to the south. (b) Contours of the mean divergence of the across-channel flow. Positive values (darker tones) indicate convergence regions (looking toward the ocean).

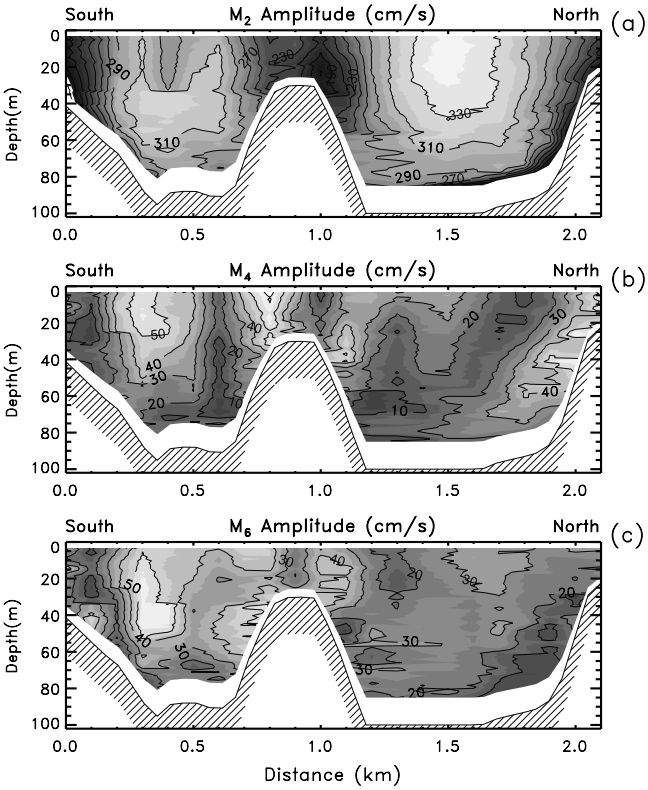

Figure 4. Across-channel tidal amplitude distributions for the (a) M_2 constituent, (b) M_4, and (c) M_6 obtained from the ADCP current measurements (looking toward the ocean).

tidal current amplitudes. Highest values of the quarter-diurnal current amplitudes were found at different locations: near surface in the southern channel, over the pinnacle, in the northern flank and in the northern slope. In the case of the sixth-diurnal tidal currents the highest values were located in the southern channel with a peak at mid-depth, in the southern flank, and around the summit of the pinnacle. It is noteworthy that the highest values of the quarter-diurnal and sixth-diurnal amplitudes overlap the surface region of the southern channel and that semi-diurnal highest values in this channel have been shifted to mid-depth. Thus the strongest overtide amplitudes were located over the pinnacle, on the slopes, and in the southern channel. The northern channel was mostly influenced by semidiurnal tidal currents. The southern channel is shallower and narrower than the northern channel and friction may play a role in determining the enhancement of overtides in the southern side. The large overtides in the southern channel may have been then caused by nonlinearities that arise from (1) increased frictional effects because of its shallowness and (2) spatial gradients in the flow at Seluian Bank to the southeast of the sampling transect.

[18] The southern channel was also characterized by larger mean velocities than the northern side (Figure 2). This could be explained by the effect of Bernoulli-type accelerations originated away from the pinnacle, possibly the Seluian Bank.

[19] In order to further explore the strength of nonlinearities through tidal asymmetries [e.g., *Speer et al.*, 1991], the phase relationship (2 M_2-M_4) and a ratio of the amplitude of the quarter-diurnal flow to the amplitude of the semi-diurnal flow (M_4/M_2) were explored. Tidal distortion was observed in the relative phase (2 M_2-M_4) shown in Figure 5. Values between 0° and 180° indicated a longer falling than rising tide and hence a tendency toward flood-dominance. Longer rising tide and ebb-dominant conditions were indicated by a (2 M_2-M_4) relative phase between 180° and 360° [*Speer et al.*, 1991]. This indicated a tendency for a flood-dominated regime over the shoals, in agreement with the mean inflow observed there. Figure 5 remarkably matches the regions of mean inflow and mean outflow in Figure 2, exhibiting a tendency to flood and ebb-dominance, respectively. The ratio of M_4 to M_2 amplitude (not plotted here) also showed the highest values over the pinnacle and over the northern slope, consistent with the mean flow. It then follows that the main characteristics of the mean flow were derived from strong tidal asymmetries as observed in these tidal patterns.

[20] Overtidal current amplitudes observed in other channel systems with tidal currents of ~1 m/s have shown that quarter-diurnal amplitudes were typically about three times larger than the sixth-diurnal amplitudes in English Channel [*Le Provost and Forferino*, 1985]. The results reported here have shown that both components exhibit comparable values, which has been rarely reported. This suggests that in the generation of the sixth-diurnal overtide there is probably a source that is less relevant in other systems but important here, such as horizontal friction. The generation of sixth-diurnal overtides of similar magnitude to fourth-diurnal overtides as well as the observed pattern of mean flows indicate the importance of friction (both horizontal and vertical) to the momentum balance, which is investigated further in the subsections dealing with the dynamics.

3.3. Salinity and Temperature Profiles

[21] In general all the stations showed a nearly vertically homogeneous water column. Figure 6 corresponds to the vertical profile of temperature and salinity CTD data obtained from a station in the deepest part of the northern channel. Stratification was very weak in the deepest water column of the section, as temperature changed by 0.2°C and salinity by 0.15 over a depth of 130 m. All profiles showed

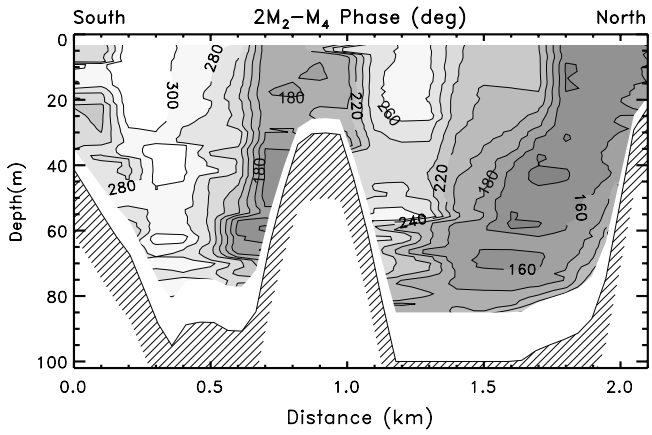

Figure 5. Across-channel distribution of the 2 M_2-M_4 phase relationship. Values below 180° suggest flood-dominance (looking toward the ocean).

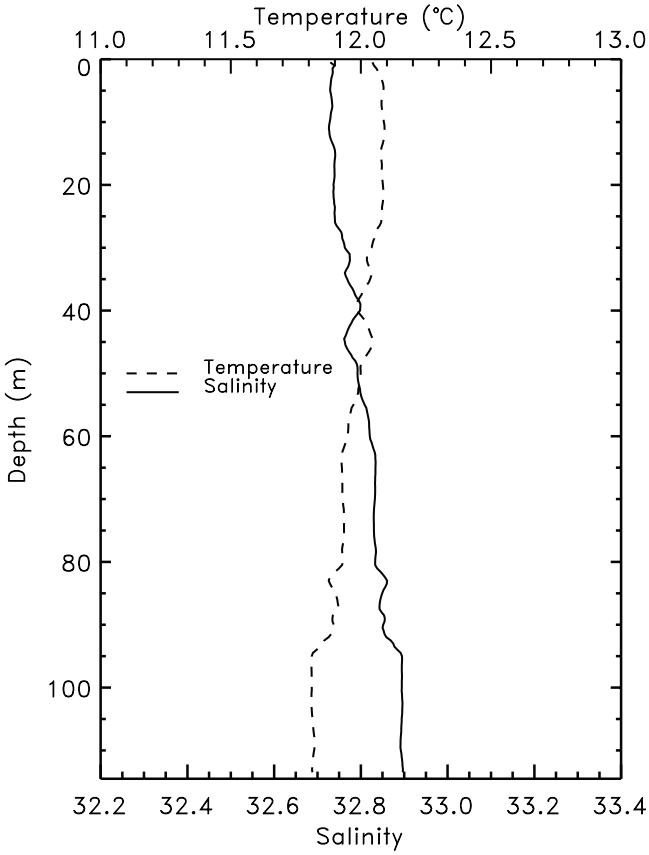

Figure 6. Salinity and temperature profiles in the deepest (−120 m) region of the northern channel. Vertical stratification is very weak and an inverse correlation between temperature and salinity is observed.

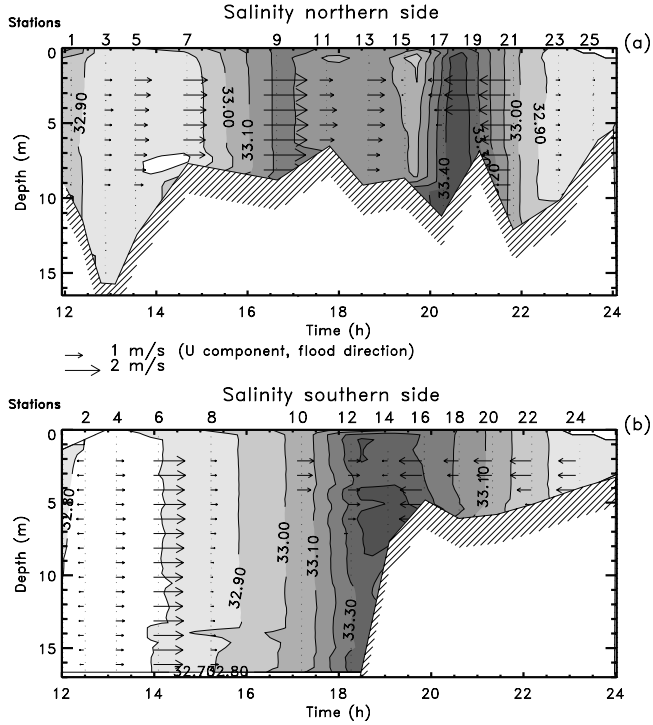

Figure 7. Time series of salinity profiles at the (a) northern and (b) southern sides. Contour interval is 0.1.

a strong correlation between temperature and salinity data (correlation coefficient of ∼0.92), indicative of near-conservative mixing. Figure 7 shows the evolution in time of the salinity field for the CTD stations in the northern and southern extremes of the transect. Current vectors are plotted on it to show the tidal phases. No vertical structure was observed, and changes in salinity seemed to respond to changes in the velocity field. Highest and lowest salinity values approximately appeared at the times of slack waters. Differences in time for maximum values of salinity appearing in the northern side relative to the southern side, were consistent with flood-dominance (northern) and ebb-dominance (southern) asymmetry shown in the relationships between the quarter-diurnal and sixth-diurnal tidal constituents (Figure 5).

3.4. Across-Channel Dynamics

[22] The across-channel distributions of the mean Coriolis term $\langle fu \rangle$, the advective term $\langle v(\partial v/\partial y) \rangle$, and the frictional terms $\langle A_z(\partial^2 v/\partial z^2) \rangle$ and $\langle A_h(\partial^2 v/\partial y^2) \rangle$ were used to establish their relative contribution to the across-channel momentum balance. Figures 8 and 9 show the distribution of the Coriolis, advective, and frictional terms. As expected, the Coriolis term (Figure 8a) resembled the u mean flow distribution (Figure 2), as it is directly proportional to it. The advective term distribution (Figure 8b) showed values almost one order of magnitude greater than those of the

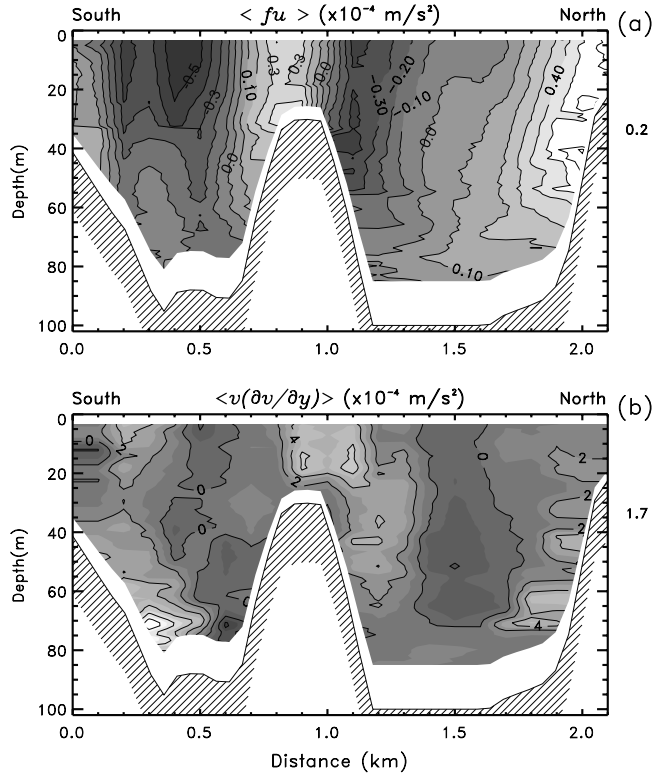

Figure 8. Contours of the mean (a) Coriolis term and (b) advective term. Looking toward the ocean.

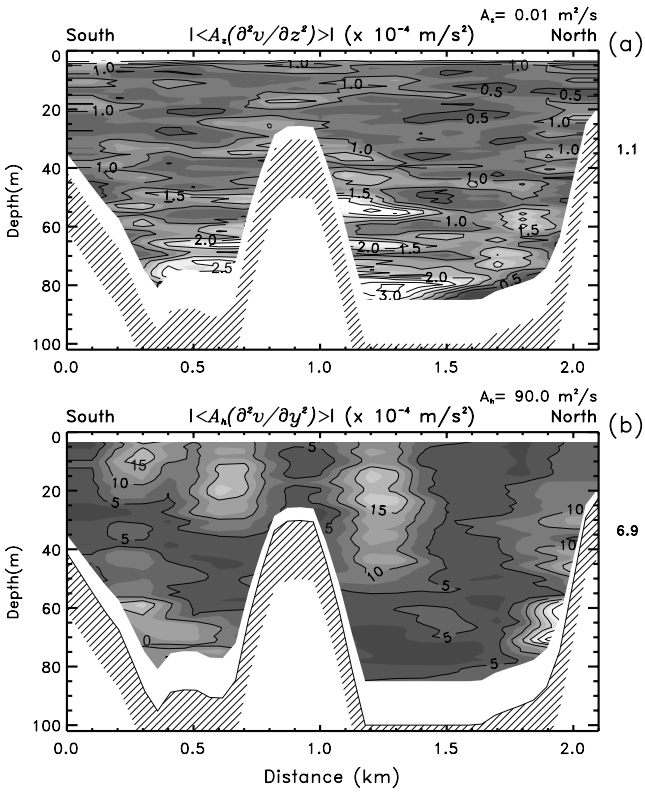

Figure 9. Contours of the mean (a) vertical frictional term and (b) horizontal frictional term. Looking toward the ocean.

Coriolis term. They were highest over the northern flank of the pinnacle and over the southern slope. The dominance of this term is derived from the extraordinarily high absolute values of the lateral convergence $|(\partial v/\partial y)|$ previously mentioned, which were typically 1.0 to 2.0 $\times$ 10^{-3}, i.e, a change of 0.1 to 0.2 m/s in just 100 m in the cross-channel direction. The vertical friction term $A_z[\partial^2 v/\partial z^2]$ (Figure 9a), which again is diagnostic owing to the constant A_z, showed the highest values not only around the flanks but also over the pinnacle and close to the bottom, as expected from bottom friction effects. This term was typically five times greater than fu (Figure 8a). In turn, the horizontal friction term $A_h[\partial^2 v/\partial y^2]$ (Figure 9b) was also strongly influenced by the changes of the v velocity component in the cross-channel direction. The greatest values appeared on both sides of the pinnacle and over the southern slope. Their magnitudes were about four times greater than those observed for the advective term (Figure 8b) and they were at least one order of magnitude greater than the Coriolis term (Figure 8a). This is a revealing result as this term is customarily neglected from the momentum balance. Although the value of A_h used here is nominal, the order of magnitude of the horizontal friction term suggests that it is important to the dynamics. This becomes evident from the marked boils and recirculations observed during the data collection, similar to those described by *Farmer et al.* [1995].

[23] Sectional means for the distributions of the absolute values of the Coriolis term, the advective term, the vertical frictional term and the horizontal frictional term were 0.22 (Figure 8a), 1.7 (Figure 8b), 1.09 (Figure 9a), and 6.88 (Figure 9b), respectively. Then the approximated relative magnitude of these terms in the y direction diagnostically becomes:

1	:	8	:	5	:	31	
Coriolis Term		Advective term		Vertical Frictional		Horizontal Frictional	(2)

The dominance of the advective term and the horizontal friction term in this balance is clearly due to the influence of the lateral divergence $\partial v/\partial y$, which was particularly high around the pinnacle and on the southern slope. This is most likely induced by the effect of the Remolinos Rocks in shaping the across-channel current distribution. Values in equation (2) also suggested that the across-channel dynamic balance is mostly between advective accelerations and friction. The baroclinic pressure gradient might not be relevant to this balance as differences in salinity (Figure 6) between both sides of the channel were low. However, the barotropic pressure gradient could be important if the transverse slopes in sea level are of the order of 10^{-5} or 1 cm in 1 km, which may be possible in this area. A spatial comparison between the Coriolis accelerations and the advective and frictional terms is presented in Figure 10. As suggested by the mean values in equation (2), the distributions show a clear dominance of frictional over Coriolis accelerations, because the ratios are greater than 1 nearly everywhere, except for spotty regions. On the other

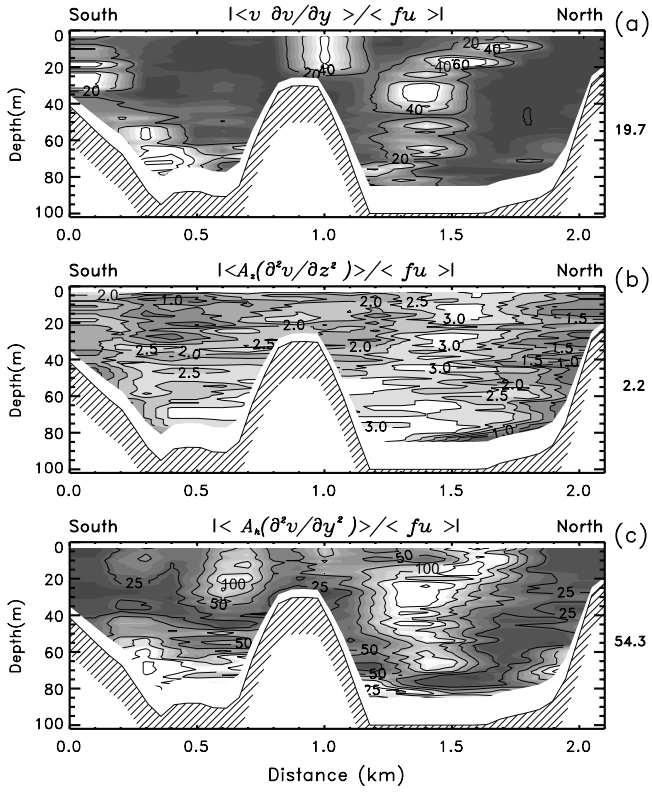

Figure 10. Ratios of the absolute values of (a) mean nonlinear term to Coriolis acceleration, (b) vertical frictional term to Coriolis acceleration, and (c) horizontal frictional term to Coriolis acceleration. Looking toward the ocean.

Table 1. Approximated Relative Magnitude of the Across-Channel Momentum Balance With Different Values of Both Vertical and Horizontal Eddy Viscosity Coefficients

	Coriolis Term	Advective Term	Vertical Frictional Term	Horizontal Frictional Term
A_h = 90 m^2/s and A_z = 0.01 m^2/s	1	8	5	31
A_h = 180 m^2/s and A_z = 0.01 m^2/s	1	8	5	62
A_h = 90 m^2/s and A_z = 0.1 m^2/s	1	8	11	31

hand, highest values in the northern channel (Figures 10a and 10c) might be attributed to the lower values of u. The distributions of the advective/Coriolis (Figure 10a) and horizontal friction/Coriolis (Figure 10c) ratios showed again the influence of the horizontal gradient $\partial v/\partial y$. It follows from Figure 10 that advective accelerations and friction (vertical and horizontal) should be important contributors to the lateral momentum balance. It is noteworthy to highlight the potential role of horizontal friction in energetic channels, as it is often neglected. Similar behavior related to horizontal friction has been observed in North Inlet, South Carolina by B. Kjerfve (personal communication, 2001).

4. Discussion

[24] In the results presented above, it has been shown that horizontal friction is one of the important terms in the across-channel momentum balance. Here this balance will be further explored and will be compared to the along-channel momentum balance.

4.1. Across-Channel Momentum Balance

[25] From equation (2) the relevant terms in the across-channel momentum balance become

$$\langle v(\partial v/\partial y)\rangle = \langle A_h(\partial^2 v/\partial y^2)\rangle + \langle A_z(\partial^2 v/\partial z^2)\rangle - \langle 1/\rho(\partial p/\partial y)\rangle \quad (3)$$

which is a balance weakly dependent in depth and strongly dependent on the variations of v in the y direction ($\partial v/\partial y$). Note that the pressure gradient term has been included because it also may contribute to the momentum balance. Otherwise, this balance could be regarded as one in which the advection of momentum is balanced by the diffusion of momentum (i.e., advection-diffusion balance). It is also noteworthy that lateral stresses are dominant over vertical stresses, although the latter are still more important than Coriolis accelerations. In addition, it is possible that the two terms $\langle u(\partial v/\partial x)\rangle$ and $\langle A_h(\partial^2 v/\partial x^2)\rangle$ that appear in equation (1) are relevant to the dynamics because of the large variability that is expected in the along-channel direction as suggested by the along-channel variations of the bathymetry.

[26] As indicated in section 2, the coefficients used for the frictional terms A_h and A_z were held constant in the balance. This was done only in the interest of simplicity and represents an approximation. The coefficients used here (A_h = 90 m^2/s and A_z = 0.01 m^2/s) are roughly the same used for the English Channel [*Pingree and Maddock*, 1978] and Juan de Fuca Strait [*Ott and Garrett*, 1998], which are both energetic (tidal currents > 1 m/s) and of similar depths to the Chacao Channel.

[27] The sensitivity of these coefficients to our results was explored using the values indicated in Table 1. When A_h is increased, the importance of the horizontal friction term increases linearly. When A_z increases one order of magnitude, the vertical frictional term becomes more important than advective accelerations in the momentum balance. Thus both parameters have some effect in the solution but the contribution of both advective accelerations and horizontal friction remains relevant. In any case, the values used in this work are considered conservative underestimates for the magnitude of the currents and the channel bathymetry in Chacao.

4.2. Along-Channel Balance

[28] The full balance may be written as

$$\langle u(\partial u/\partial x)\rangle + \langle v(\partial u/\partial y)\rangle + \langle w(\partial u/\partial z)\rangle - \langle fv\rangle = -\langle 1/\rho(\partial p/\partial x)\rangle + \langle A_h(\partial^2 u/\partial x^2)\rangle + \langle A_h(\partial^2 u/\partial y^2)\rangle + \langle A_z(\partial^2 u/\partial z^2)\rangle. \quad (4)$$

The strong divergences documented above are expected to be linked to large lateral shears ($\partial u/\partial y$) [*Valle-Levinson et al.*, 2003], which might translate into the importance of advective terms (e.g., $v\partial u/\partial y$) to the along-channel momentum balance. To explore this we can see that the distributions of ($\partial v/\partial y$) (Figure 3b) and ($\partial u/\partial y$) (Figure 11) coincide with their corresponding regions of maximum and minimum, although the values of ($\partial u/\partial y$) are typically three times those of ($\partial v/\partial y$). In particular, the southern slope and both flanks of the pinnacle are regions where the strongest lateral shears and divergences are observed. Thus analogously to the across-channel momentum balance, the relevance of lateral shears seem to be also important to the along-channel momentum balance. The along-channel pressure gradients should then be balanced by advection and friction because the terms reliably computed $\langle fv\rangle$;,

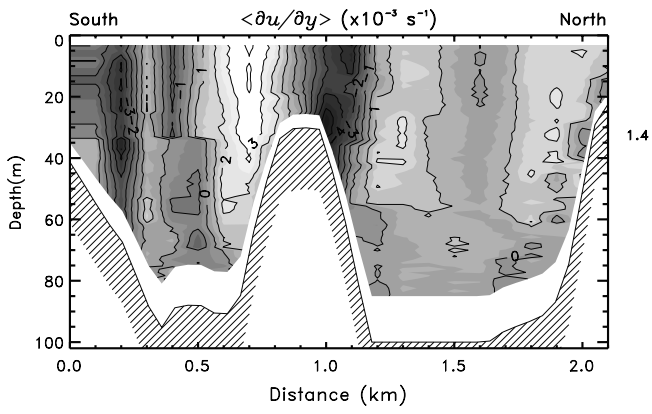

Figure 11. Contours of the mean lateral shear of the along-estuary flow. Lighter shades indicate positive shears (negative vorticity) and darker shades represent negative shears (positive vorticity). Looking toward the ocean.

$\langle v(\partial u/\partial y)\rangle$, $\langle A_z[\partial^2 u/\partial z^2]\rangle$ and $\langle A_h[\partial^2 u/\partial y^2]\rangle$ show sectional means (not plotted here) of 0.1, 5.1, 1.2, and 14.7 ($\times 10^{-4}$), respectively. The approximate relative magnitude of the terms in the along-channel dimension becomes

1	:	50	:	10	:	150	
Coriolis Term		Advective Term		Vertical Frictional		Horizontal Frictional	(5)

Again, the magnitude and distribution of the lateral shears of velocity $\partial u/\partial y$ (Figure 11) are potentially playing a key role in this behavior. Another way to conceptualize the relevance of the along-channel variability is to consider that the advective acceleration $u(\partial u/\partial x)$ may be scaled as U^2/L_x where U = 2 m/s and L_x = 5000 m. In this case, the advective term will be 8×10^{-4} and will balance the mean of the lateral friction term $A_h[\partial^2 u/\partial y^2]$, estimated at $\sim 11.4 \times 10^{-4}$. Then in the along-channel momentum balance advective accelerations and friction (both lateral and vertical) are important contributors to the dynamics.

[29] *Friedrichs and Madsen* [1992] investigated the magnitudes of advective accelerations relative to friction in 13 estuaries with different depths, tidal ranges, and typical tidal velocities. They found the greater values (>1) of these ratios in deeper estuaries (40 m), as bottom friction becomes less important. In contrast, the ratios advective/(bottom friction + horizontal friction) for the present work were 0.2 (across-channel) and 0.3 (along-channel), obtained from equations (2) and (5), respectively, which once more show the relevance of horizontal friction to the dynamic balance. These ratios support the idea that in energetic and bathymetrically complex channels, such as Chacao Channel, horizontal friction plays a key role in the momentum balance.

[30] It is noteworthy that the mean flows in Chacao Channel were consistent with the theoretical results of *Li and O'Donnell* [1997] even though they may be caused by different mechanisms. In the theoretical results, the transverse distribution of along-estuary flows is attributed mostly to the Stokes drift, i.e., correlation between u and sea level. The observations in Chacao Channel and North Inlet suggest that fricitonal effects may be responsible too. Nonetheless, Stokes drift and friction both are nonlinear mechanisms that induce asymmetries in the tidal flows that generate mean flows. Therefore we propose that horizontal friction, through lateral gradients in the tidal flows, is another plausible mechanism that generates the pattern of observed mean flows. This is supported by (1) the spatial distribution of the relative phases between semidiurnal tidal currents and overtides (2 M_2-M_4, Figure 5), which reflects asymmetries that explain the mean flow patterns and (2) the marked effects of horizontal friction on the mean dynamics.

5. Conclusion

[31] This study of flow over a pinnacle in an energetic tidal channel features a mean flow pattern consisting of recirculation around the pinnacle and over the slopes of the channels that resemble theoretical results [e.g., *Park*, 1990; *Li and O'Donnell*, 1997], as illustrated by the schematic diagram presented in Figure 12. Under the influence of lateral variations of bathymetry, the mean flow is flood dominated at all depths in shallow areas and ebb dominated in the deeper areas of the same cross section. These recirculations reflect strong divergences and lateral shears that translate into a relevant contribution of the nonlinear terms (advection, horizontal, and vertical friction) to the momentum balance. In particular, this study highlights the prominence that horizontal friction may exert on the dynamics of an energetic tidal channel. This constitutes one of the few reported examples where horizontal friction may be relevant to the dynamics of a naturally occurring flow. Some of the results presented here might be also important in studies of dispersion of particulated material in the region.

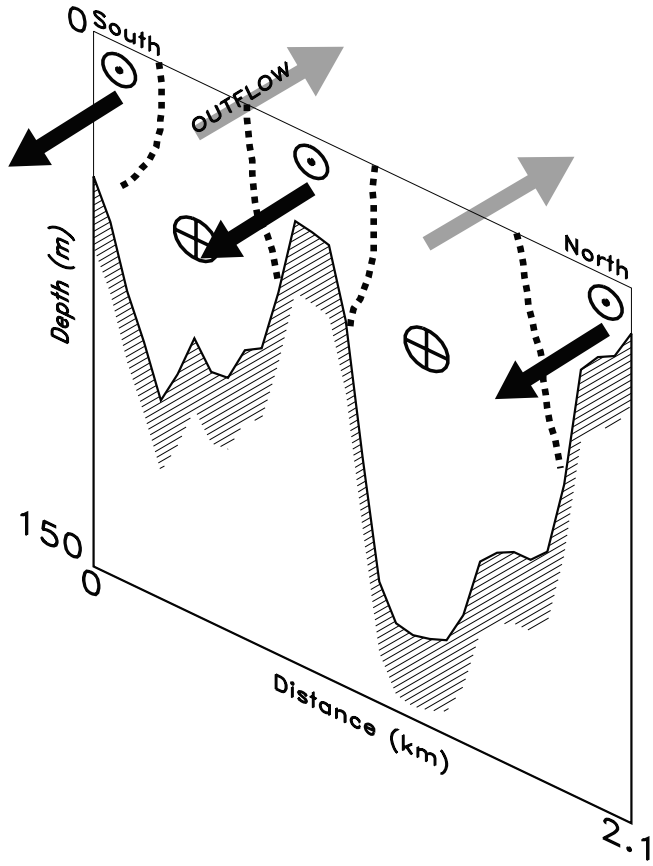

Figure 12. Schematic representation of the along-channel mean flow across the channel. Outflow (gray arrows) and inflow (black arrows) regions are separated by strong convergences or lateral shears represented by the dashed lines.

[32] **Acknowledgments.** This project was funded by the U.S. National Science Foundation under project NSF-INT-9625934. Thanks to Hector A. Sepulveda, Wolfgang Schneider, Dante Figueroa, and Ricardo De Pol who participated in the field work. Ariel Gallardo provided the transportation to the sampling site. The Servicio Meteorológico de la Armada (Meteorological Service of the Chilean Navy) provided the meteorological data for the general description of the region.

References

Bowden, K. H., and P. Hamilton, Some experiments with a numerical model of circulation and mixing in a tidal estuary, *Estuarine Coastal Shelf Sci.*, *3*, 281–301, 1975.

Cameron, W. M., On the transverse forces in British Columbia inlet, *Trans. R. Soc. Can.*, *45*, 1–9, 1951.

Chapman, D. C., and D. B. Haidvogel, Formation of Taylor caps over a tall isolated seamount in a stratified ocean, *Geophys. Astrophys. Fluid Dyn.*, *64*, 31–65, 1992.

Csanady, G. T., Lateral momentum flux in boundary currents, *J. Phys. Oceanogr.*, *5*, 705–717, 1975.

Defant, A., *Physical Oceanography*, vol. 2, 598 pp., Pergamon, New York, 1961.

Dyer, K., *Estuaries: A Physical Introduction*, 2nd ed., 195 pp., John Wiley, New York, 1997.

Farmer, D., E. D'Asaro, M. Trevorrow, and G. Dairiki, Three-dimensional structure in a tidal convergence front, *Cont. Shelf Res.*, *15*(13), 1649–1673, 1995.

Friedrichs, C., and O. Madsen, Nonlinear diffusion of the tidal signal in frictionally dominated embayments, *J. Geophys. Res.*, *97*(C4), 5637–5650, 1992.

Geyer, W. R., J. Trowbridge, and M. Bowen, The dynamics of a partially mixed estuary, *J. Phys. Oceanogr.*, *30*, 2035–2048, 2000.

Le Provost, C., and M. Forferino, Tidal Spectroscopy of the English Channel with a numerical model, *J. Phys. Oceanogr.*, *15*, 1009–1031, 1985.

Li, C., and J. O'Donnell, Tidally driven residual circulation in shallow estuaries with lateral depth variation, *J. Geophys. Res.*, *102*(C13), 27,915–27,929, 1997.

Lwiza, K. M. M., D. G. Bowers, and J. H. Simpson, Residual and tidal flow at a tidal mixing front in the North Sea, *Cont. Shelf Res.*, *11*(11), 1379–1395, 1991.

Park, M.-J., Transient tidal vorticity in coastal seas, Ph.D thesis, 105 pp., State University of New York at Stony Brook, Stony Brook, N. Y., 1990.

Parker, B. B., The relative importance of the various nonlinear mechanisms in a wide range of tidal interactions, in *Tidal Hydrodynamics*, edited by B. B. Parker, pp. 237–268, John Wiley, New York, 1991.

Ott, M. W., and C. Garrett, Frictional estuarine flow in Juan de Fuca Strait, with implications for secondary circulation, *J. Geophys. Res.*, *103*(C8), 15,657–15,666, 1998.

Pingree, R. D., and L. Maddock, The M4 tide in the English Channel derived form a nonlinear numerical model of the M_2 tide, *Deep Sea Res.*, *25*, 53–63, 1978.

Pond, S. and G. L. Pickard, *Introductory Dynamical Oceanography*, 3rd ed., 329 pp., Pergamon, New York, 1998.

Redfield, A. C., *Introduction to the Tides*, 340 pp., Mar. Sci. Int., Woods Hole, Mass., 1980.

SHOA, Canal Chacao, *Nautical Chart 7210*, 5th ed., Hydrogr. and Oceanogr. Serv. of Chilean Navy (SHOA), Valparaíso, Chile, 1993.

SHOA, Derrotero de la costa de Chile, *Pub. 3001*, 8th ed., vol. I and II, Hydrogr. and Oceanogr. Serv. of Chilean Navy (SHOA), Valparaíso, Chile, 1995.

Smith, R., Combined effects of buoyancy and tides upon longitudinal dispersion, in *Bouyancy Effects on Coastal and Estuarine Dynamics, Coastal Estuarine Stud.*, vol. 53, edited by D. Aubrey and C. Friedrichs, pp. 319–329, AGU, Washington, DC, 1996.

Speer, P. E., D. Aubrey, and C. Friedrichs, Nonlinear hydrodynamics of shallow tidal inlet/bay systems, in *Tidal Hydrodynamics*, edited by B. B. Parker, pp. 321–339, John Wiley, New York, 1991.

Tee, K. T., Tide-induced residual current, a 2-D nonlinear numerical tidal model, *Journal of Marine Research*, *34*, 603–628, 1976.

Tully, J. P., On structure, entrainment and transport in estuarine embayments, *J. Mar. Res.*, *17*, 523–535, 1958.

Trump, C. L., and G. Marmorino, Calibrating a gyrocompass using ADCP and DGPS data, *J. Atmos. Ocean. Technol.*, *14*, 211–214, 1997.

Valle-Levinson, A., and L. P. Atkinson, Spatial gradients in the flow over an estuarine channel, *Estuaries*, *22*(2A), 179–193, 1999.

Valle-Levinson, A., W. C. Boicourt, and M. Roman, On the linkages among density, flow, and bathymetry gradients at the entrance to the Chesapeake Bay, *Estuaries*, in press, 2003.

Walters, R. and F. Werner, Nonlinear generation of overtides, compound tides, and residuals, in *Tidal Hydrodynamics*, edited by B. Parker, pp. 297–320, John Wiley, New York, 1991.

Wells, J. T., Dynamics of coastal fluid muds in low-moderate-, and high-tide-range environments, *Can. J. Fish. Aquatic Sci.*, *40*, suppl. 1, 130–142, 1983.

L. Atkinson and A. Valle-Levinson, Center for Coastal Physical Oceanography, Department of Ocean, Earth, and Atmospheric Sciences, Old Dominion University, Norfolk, VA 23529, USA. (atkinson@ccpo.odu.edu; arnoldo@ccpo.odu.edu)

M. Cáceres, Servicio Hidrografico y Oceanografico de la Armada, Ervazuriz 232, Valparaiso, Chile. (div.tecnica02.oc@shoa.cl)